# Evaluating some design criteria for TiFe-based ternary hydrogen storage alloys

Nayebossadri, Shahrouz; Greenwood, Carmel; Book, David

Link to publication on Research at Birmingham portal

# Evaluating some design criteria for TiFe-based ternary hydrogen storage alloys

Shahrouz Nayebossadri *, Carmel Jenjira Greenwood, David Book

*School of Metallurgy and Materials, University of Birmingham, Edgbaston, Birmingham B15 2SE, UK*

## ARTICLE INFO

## ABSTRACT

Elemental substitution is widely practised to fabricate TiFe-based alloys with enhanced hydrogen storage characteristics. While some hydrogen storage properties can be improved others are usually adversely affected by this method. Hence, establishing sensible alloying design criteria is important for further developing Ti-Fe-based alloys. Here, the effects of substitutional elements in Ti-Fe-based ternary alloys are assessed based on several factors such as hydrogen bond dissociation energy, lattice parameters, interstitial site size, and intermetallic phase formation. Our calculations show that all the substitutional elements studied in this work (except Ni and Co) increase the lattice parameter compared to the TiFe alloy, while they have a diverse effect on the interstitial site sizes. The thermodynamic stability of the alloys could not be adequately described based on the lattice parameter and factors such as interstitial site sizes along the local atomic environment should be also considered. Hydrogen storage capacity of the Ti-Fe-based ternary alloys also appears to be influenced by the metal-hydrogen bond dissociation energy of the substitutional elements and their capability to form intermetallic phases with Ti. TiFe-based ternary alloys were modified by V and Zr substitutions according to the above criteria. The modified alloys were mostly composed of the B2 TiFe phase, offering significantly easier activation and a higher reversible hydrogen storage capacity compared to the binary alloy.

## 1. Introduction

AB alloys are promising candidates for stationary hydrogen storage applications since gravimetric capacity is less important compared to mobile applications. Ti(A site)Fe(B site) is the most well-known alloy in this class of hydrides and crystallises in an ordered body-centred cubic, CsCl-type structure corresponding to Pm-3 m space group with a lattice parameter of 2.98 Å [1]. TiFe is particularly appealing because of its reasonable maximum storage capacity of approximately 1.9 wt% H [2], low raw material cost and moderate conditions for reversible hydrogen absorption/desorption. According to the Ti-Fe phase diagram (Figure SI1), two intermetallic phases form including TiFe and TiFe$_2$. While TiFe (B2 TiFe) phase absorbs hydrogen, the TiFe$_2$ phase with C14 Laves structure does not absorb hydrogen.

However, TiFe has a number of drawbacks such as the practical application of TiFe produced through conventional metallurgical methods is hampered by its complicated and lengthy activation procedure [2], and sensitivity to gaseous impurities in hydrogen following the activation procedure [3].

Activation treatments that cycle through elevated temperatures and hydrogen pressures cause expansion and contraction in the lattice, exposing fresh, non-oxidised surfaces upon which hydrogen can interact. Several activation mechanisms have been proposed including surface segregation with Fe-rich cluster formation, oxide layer dissolution, formation of lattice cracks and FeTiO$_x$ suboxides acting as catalysts. Sandrock et al. [4] showed the bulk and surface compositions of un-activated TiFe were similar whereas, after numerous hydrogenation and dehydrogenation cycles, oxygen-induced segregation occurred, leading to different bulk and surface compositions. The surface appeared to be rich in titanium whilst the layer immediately beneath was titanium deficient. An increase in magnetic susceptibility after hydrogenation led Schlapbach et al. [5] to suggest that in addition to segregation, magnetic Fe clusters formed near the surface and possibly in the bulk, acting as catalytic sites for hydrogen dissociation. Nevertheless, the analysis of TiFe alloy annealed in varying partial pressures of oxygen and hydrogen using TEM [6] did not find evidence of Fe clusters. Instead, surface oxide dissolution occurred, and other catalytically active molecules were present.

---

* Corresponding author.
*E-mail address:* s.nayebossadri@bham.ac.uk (S. Nayebossadri).

Edalati et al. [7] showed high-pressure torsion, a severe plastic deformation method can also improve atomic hydrogen diffusion required for activation regardless of temperature. This allowed hydrogen absorption in TiFe without the need for activation using heat treatment. They suggested that the enhanced atomic hydrogen diffusion occurred through the surface segregation of Fe-rich islands beneficial to hydrogen dissociation and the formation of significant quantities of lattice defects including cracks and grain boundaries, creating accessible atomic hydrogen diffusion paths from the surface to the interior.

Evidence for easier activation (lower $H_2$ pressure required) with decreasing grain size, and therefore higher volume of high-angle grain boundaries, was also seen in other studies [8,9], indicating the role of grain boundaries in assisting hydrogen absorption and desorption kinetics in TiFe.

Secondary phases formed in the off-stoichiometry TiFe alloys such as oxygen-stabilised intermetallics $Ti_{10}Fe_7O_3$ or β-Ti (due to excess titanium or oxygen) were also reported [4,10–13] to aid with activation by lowering alloy fracture toughness, increasing brittleness and decrepitation, and acting as preferential sites for hydride nucleation and growth [5].

Compositional modifications were also used to modify activation behaviour as well as hydrogen storage properties of the TiFe alloy. Attempts to improve activation have been undertaken through either adjusting Ti/Fe ratios in the binary system or alloying additions. In the binary alloy, the B2 TiFe phase has a stoichiometry range of 49.8–52.5 at% Ti (see Figure SI1). Increasing alloy titanium content led to a higher volume fraction of β-Ti and decreasing grain size of TiFe alloy [13,14]. TiFe lattice parameters increased from 2.977 Å in TiFe to 2.989 Å in $Ti_{67}Fe_{33}$, most likely due to the dissolution of excess titanium. In both studies, activation occurred at room temperature under 30–40 bar $H_2$ for all alloys except for the stoichiometric TiFe alloy. These methods help by providing new pathways for hydrogen transport, such as through grain boundaries, or easier dissociation of surface $H_2$ molecules.

The effects of alloying additions on hydrogen storage properties of TiFe have been also extensively studied. Some of the previous investigations exploring the effects of elemental substitutions in A, B or AB sites on the hydrogen storage properties and the activation behaviour of cast TiFe alloys are summarised in Table 1. Often, modifying one storage property through composition will affect other properties, sometimes adversely. The narrow stoichiometry range of the B2 TiFe phase and sensitivity to oxygen also means TiFe-based alloys usually have a multiphase nature which complicates hydrogen interaction.

Therefore, identifying suitable alloying additions and establishing sensible design criteria for TiFe-based ternary alloys are important for enhanced hydrogen storage characteristics. In this work, the effects of some substitutional elements on the lattice parameters and interstitial site sizes in the TiFe-based ternary alloys will be theoretically examined. We will then fabricate and study the effects of some design criteria such as hydrogen bond dissociation energies, lattice parameters, and interstitial site sizes on the hydrogen storage properties of TiFe-based ternary alloys.

## 2. Experimental

### 2.1. Starting materials and alloys synthesis

Samples were prepared by arc-melting bulk and powdered starting materials. Elemental starting materials, their form and suppliers are detailed in Table 2. All samples were 6 g and weighed out in the appropriate elemental ratios on a balance with 0.1 mg accuracy. These were loaded into a homebuilt arc melt system onto a water-cooled copper hearth. The chamber was evacuated to $10^{-2}$ mbar using a rotary vacuum pump and filled with argon (99.998%);

this process was repeated five times. Before melting each sample, a sacrificial zirconium getter was melted to remove residual oxygen remaining in the chamber. Each sample was melted three times using a 70 A current and turned over between each melt to ensure the complete melting of starting materials. Samples were left to fully cool before removing from the chamber.

### 2.2. Microstructural and compositional evaluations

Samples were prepared for microstructural characterisation by taking cross sections of cast buttons which were then mounted in conducting bakelite, ground and polished. Back scattered electron micrographs were taken from unetched specimens while secondary electron micrographs were taken from specimens etched with Keller's reagent.

Morphological and chemical characterisation was performed by Jeol 6060LV SEM equipped with an Oxford Instruments EDS detector and Inca software. Overall alloy and phase compositions were determined from the area and point scans respectively, both from a minimum of five measurements at different areas on the sample. Chemical analysis to determine alloy composition and oxygen content was carried out using ICP-OES and Leco from AMG Analytical Services. Nominal and measured compositions of alloys in this study are detailed in Table 3.

### 2.3. Structural characterisations

Samples were prepared for XRD by crushing arc melted buttons into a powder in a glovebox. The crushed powder was then sieved to collect particles with sizes between 75 and 150 μm. Structural characterisation at room temperature was carried out using a Proto benchtop diffractometer using the following parameters: Cu target with Ni filter, 1 mm slit, 0.014° step size, 10 s step time. Rietveld refinement was performed using Topas Academic and jEdit software [43].

### 2.4. Characterisation of hydrogen storage properties

Pressure-Composition-Isotherms (PCI) measurements were performed using a commercial volumetric Sieverts system by Hiden Isochema. Samples were prepared by crushing arc melted buttons into a powder in a glovebox and sieved to collect particles with sizes between 75 and 150 μm. Samples were stored and loaded inertly to prevent oxidation. Activation was performed in-situ before PCI measurements using sequences detailed in Table 4.

After activation, PCI measurements were performed in isotherm mode between 0 and 80 bar $H_2$ in 5 bar increments at 25, 40, 60 and 80 °C. Smaller steps of 0.5 bar were used for the absorption and desorption plateaux. Two PCIs were performed at each temperature and a hold time of 20 min for each pressure step was used. Kinetics of each isotherm were checked to ensure hold times were sufficiently long. In the case of alloys 1 pressure steps hold times were adjusted to 45 min to allow full absorption and desorption.

## 3. Results and discussion

### 3.1. Ternary alloy design criteria

To identify suitable elemental additions, the relationship between maximum hydrogen storage capacity (collated from literature) and their metal hydrogen (M-H) bond dissociation energies is examined in Fig. 1. These were separated into three groups based on the quantity of elemental additions (< 5 at%, 5 at%, and > 5 at%), with the third group (> 5 at%) ranging from 7.5 to 25 at%. Most data across all groups were for B site substitution, followed by AB site substitution which was mostly limited to < 5 at% additions. Only one

**Table 1**
Effects of alloying additions on hydrogen storage properties of cast TiFe. When stated activation is not required this refers to activation but subsequent absorption. Kinetics do not refer to activation but subsequent absorption.

| Element | Site | Addition (at%) | H Capacity (wt%) | Temperature (°C) | Effects | Reference |
|---|---|---|---|---|---|---|
| Al | B | 1.2–1.25 | 1.05–1.35 | 25–50 | Single phase with up to 5 at% Al addition; greater slope, lower plateau pressure, single plateau is seen; lower capacity; activation not required. | [4,14,15] |
| S | B | 0.97 | 1.36 | 25 | Slope decreases and plateau increases with S addition, but both are lower than TiFe; improved cyclability; activated at 373 K for 1 at% S addition but requires increasing temperature with more S. | [16] |
| V | B | 2.50 | 1.7–1.88 | 25–40 | Formation of multiple Ti-rich phases; greater slope, lower plateau, less hysteresis; higher capacity; faster kinetics; activation not required. | [17,18] |
| Cr | B | 2.5–10 | 1.13–1.85 | 40–150 | Greater slope, lower plateau; higher capacity with increasing Cr but lower than TiFe; faster kinetics; activated at 473 K under 30 bar $H_2$. | [17,19–21] |
| Mn | B | 2.5–15 | 1.3–1.9 | 5–45 | Greater slope, lower plateau; lower capacity; faster kinetics; activation was mixed where some absorbed without prior treatment and others didn't. | [19,21–24] |
| Mn | AB | 0.9–5.4 | 1.2–1.8 | 25 | Activation not required, incubation time depends on Mn content. | [26] |
| Co | B | 5–25 | 1.1–1.79 | 20–150 | Greater slope, lower plateau; lower capacity; activation not required. | [14,17,19,27] |
| Ni | B | 2.5–10 | 0.96–1.48 | 25–50 | Greater slope, lower plateau, γ definition is lost; lower capacity; activation not required. | [14,20,28–30] |
| Ni | AB | 3.41 | 0.625 | 40 | Higher volume fraction of $TiFe_2$; greater slope, lower plateau; lower capacity; activation not required. | [31] |
| Cu | B | 5.00 | 1.20 | 40 | Lower plateau; lower capacity. | [17] |
| Y | AB | 3–4 | 1.15–1.3 | 25 | Higher volume fraction of β-Ti; isotherms not provided but states capacity decreases with Y addition however, kinetic curves show capacity increasing with Y; activation not required. | [32] |
| Zr | A | 2.7–5 | 1.25–1.9 | 25 | Greater slope, lower plateau, loss of plateau definition; lower capacity, evidence of retained H due to $ZrH_2$ stabilisation; activation not required. | [33,34] |
| Zr | AB | 3.1–3.5 | 1.3–1.4 | 25 | Greater slope, lower plateau; lower capacity; activation required depending on at% addition. | [34–36] |
| Zr | B | 2.90 | 1.4 | 25 | Greater slope, lower plateau; lower capacity but higher than A or AB substitution; activation not required. | [34,37] |
| Nb | B | 2–5 | 1.75 – 2.02 | 25 | Lower plateau; lower capacity; activation not required. | [12,38] |
| Nb | A | 2–6 | 1–1.2 | 25 | Greater slope, lower plateau, higher γ plateau; lower capacity; slightly faster kinetics; activation not required. | [39] |
| Mo | B | 5.00 | 1.73 | 40 | Lower plateau; lower capacity. | [17] |
| Pd | B | 2.5–10 | 1.59–1.65 | 25 | Slope unchanged, lower β plateau, higher γ plateau than TiFe but doesn't change capacity with Pd addition; lower capacity; activated at 453 K under 35 bar $H_2$. | [40,41] |
| La | AB | 0.96–1.89 | 3.58–3.59 | 25 | Greater slope, lower plateau, less hysteresis; greater capacity than TiFe but doubling La content didn't change capacity; activation not required. | [42] |

**Table 2**
Starting materials specifications and suppliers.

| Element | Form | Purity | Supplier |
|---|---|---|---|
| Ti | Rod, 6.5 mm | 99.7% | Sigma-Aldrich |
| Ti | Powder, 150 µm | 99.5% | Goodfellow |
| Fe | Chips | 99.98% | Sigma-Aldrich |
| Fe | Powder, 60 µm | 99.0% | Goodfellow |
| V | Turnings | 99.7% | Sigma-Aldrich |
| Zr | Wire, 0.5 mm | 99.2% | Goodfellow |

**Table 3**
Nominal and measured compositions of alloys in this study, along with their identifiers. Errors associated with ICP-OES (Ti,Fe,M:1%) and Leco (O:5%).

| System | Alloy | Nominal | Measured |
|---|---|---|---|
| **Ti-Fe** | 1 | $Ti_{50}Fe_{50}$ | $Ti5_{0.9}Fe_{49.1}O_{0.18}$ |
| | 2 V | $Ti_{50}Fe_{48.8}V_{1.2}$ | $Ti_{50.6}Fe_{48.0}V_{1.4}O_{0.18}$ |
| **Ti -Fe-V** | 3 V | $Ti_{50}Fe_{46.9}V_{3.1}$ | $Ti_{50.5}Fe_{46.3}V_{3.2}O_{0.18}$ |
| | 4 V | $Ti_{50}Fe_{43.7}V_{6.3}$ | $Ti_{50.7}Fe_{42.8}V_{6.5}O_{0.18}$ |
| **Ti-Fe-Zr** | 5Zr | $Ti_{49.87}Fe_{49.87}Zr_{0.26}$ | $Ti_{50.6}Fe_{49.3}Zr_{0.15}O_{0.18}$ |

**Table 4**
Activation procedure and the number of cycles required for each alloy.

| Alloy | Sequence | Number of Cycles |
|---|---|---|
| **1** | 1. Heat to 350 °C in vacuum<br>2. Introduce 7 bar $H_2$ and hold for 30 min<br>3. Evacuate and leave to cool until room temperature<br>4. Introduce 70 bar $H_2$ and hold for 10 min<br>5. Evacuate | 4 |
| **2 V, 3 V** | 1. Heat to 100 °C and introduce 150 bar $H_2$, hold for 60 min<br>2. Evacuate | 2 |
| **5Zr** | 1. Heat to 100 °C and introduce 150 bar $H_2$, hold for 60 min<br>1. Evacuate | 1 |

data point for Zr, situated in the first group, was for A site substitution. This distribution of site substitution is expected given that A and AB site substitutions reduce hydrogen storage capacity through the formation of secondary phases [34,35]. M-H bond dissociation energies ranged from approximately 190 to 350 kJ mol⁻¹. In the first, second and third groups, the alloys with the highest storage capacity contained V [18], Nb [12], and Cr [17] additions respectively.

The worst performers in all three groups were Ti-Fe alloys with nickel additions.

Fig. 1 suggests that for additions of 5 at% or less, the best elements for maximising capacity are vanadium and niobium. The relationship where storage capacity falls with increasing M-H bond dissociation energy is a particularly good fit for B site substitution in the first group. This relationship still holds for the second group, although the data points are more scattered. It is unclear whether this is applicable to the third group, therefore moving forward, selection of compositions will be limited to alloying additions of 5 at% or less. Furthermore, greater quantities of alloying additions will lead to alloy Ti/Fe ratios greater than 1:1 potentially encourage the formation of non-absorbing phases.

In terms of M-H bond dissociation energy, maximum storage capacity peaks where this is approximately 220 kJ mol⁻¹ and movement in either direction from this value decreases capacity. Both vanadium and niobium have higher M-H bond dissociation energies relative to Ti-H and Fe-H (205 and 148 kJ mol⁻¹ respectively). However, beyond 220 kJ mol⁻¹ it seems that capacity falls, possibly because hydrogen reacts preferentially with the alloying addition and binds too tightly, potentially causing incomplete desorption.

Inspection of the first and second groups also suggests that the maximum storage capacity depends on the capability of the elemental addition forming intermetallic phases with titanium. Alloys containing chromium, copper, or aluminium additions, amongst others, generally suffered from lower capacities. These elements can form various intermetallic phases with titanium. Even when the quantities of such elements are not enough to form intermetallic phases, their presence still affects the bonding between titanium and hydrogen by moving electron density away from titanium. On the other hand, elements such as molybdenum, vanadium and niobium have large solid solubility ranges in titanium and do not form intermetallic phases.

A correlation between interstitial sizes in AB and AB₅ alloys and their corresponding hydride stabilities were established [44], where hydride stability increases with interstice size. Similarly, the plateau pressure in TiFe alloy depends directly on B2 TiFe phase lattice parameters, where larger cell sizes lead to lower plateaux [45]. To better understand the effects of alloying additions on the hydride stability and the ease of hydrogen filling in different interstitial sites, lattice parameters, octahedral and tetrahedral interstice sizes are theoretically calculated for ternary alloys (see Supporting Information). Three compositions were considered where M is the
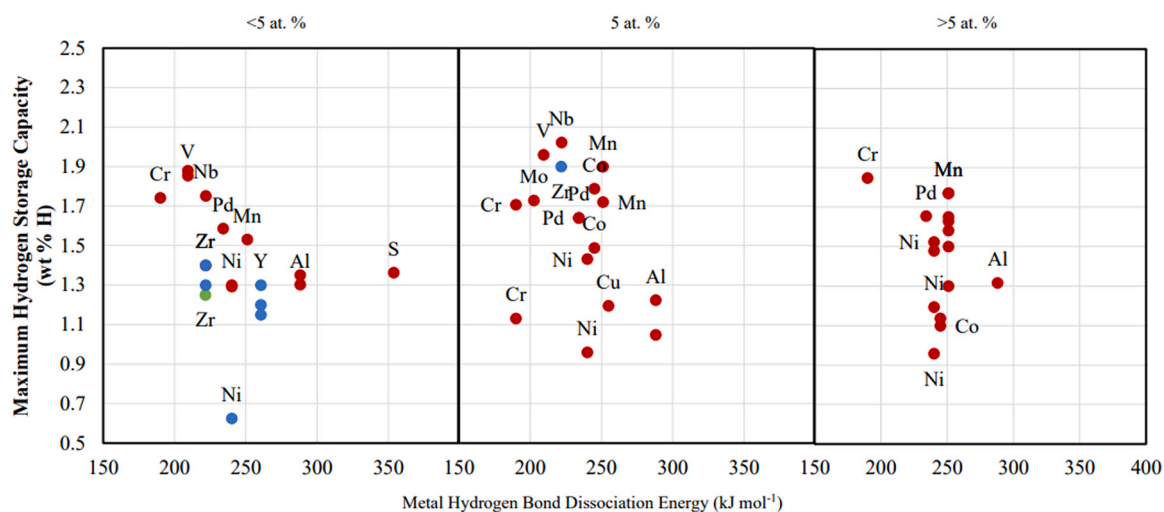


**Fig. 1.** Scatter plots of maximum storage capacities (see Table SI 1 in Supporting Information) and their associated M-H bond dissociation energies [59,60] in Ti-Fe-M alloys. Colour coded according to the site of substitution (A: green; B: red; AB: blue).

**Table 5**

Calculated lattice parameters and octahedral and tetrahedral site sizes for $TiFe_{0.964}M_{0.038}$ (1.9 at% M), $TiFe_{0.874}M_{0.126}$ (6.3 at% M) and $TiFe_{0.750}M_{0.250}$ (12.5 at% M) with various alloying additions.

| Elements | Lattice Parameter (nm) | | | Octahedral Diameter (nm) | | | | | | Tetrahedral Diameter (nm) | | |
|---|---|---|---|---|---|---|---|---|---|---|---|---|
| | 1.9% | 6.3% | 12.5% | 1.9% | | 6.3% | | 12.5% | | 1.9% | 6.3% | 12.5% |
| | | | | OM-Fe | OFe-Fe | OM-Fe | OFe-Fe | OM-Fe | OFe-Fe | | | |
| Al | 0.322 | 0.325 | 0.3349 | 0.058 | 0.070 | 0.056 | 0.073 | 0.066 | 0.083 | 0.112 | 0.115 | 0.126 |
| V | 0.318 | 0.320 | 0.3245 | 0.061 | 0.066 | 0.060 | 0.068 | 0.064 | 0.072 | 0.108 | 0.110 | 0.115 |
| Cr | 0.316 | 0.316 | 0.3175 | 0.063 | 0.064 | 0.062 | 0.064 | 0.064 | 0.066 | 0.105 | 0.106 | 0.107 |
| Mn | 0.316 | 0.316 | 0.3164 | 0.063 | 0.064 | 0.063 | 0.064 | 0.063 | 0.064 | 0.105 | 0.105 | 0.106 |
| Co | 0.315 | 0.315 | 0.3141 | 0.064 | 0.063 | 0.064 | 0.063 | 0.063 | 0.062 | 0.104 | 0.104 | 0.103 |
| Ni | 0.314 | 0.314 | 0.3129 | 0.064 | 0.062 | 0.064 | 0.062 | 0.063 | 0.061 | 0.104 | 0.103 | 0.102 |
| Cu | 0.316 | 0.316 | 0.3175 | 0.063 | 0.064 | 0.062 | 0.064 | 0.064 | 0.066 | 0.105 | 0.106 | 0.107 |
| Zn | 0.318 | 0.320 | 0.3245 | 0.061 | 0.066 | 0.060 | 0.068 | 0.064 | 0.072 | 0.108 | 0.110 | 0.115 |
| Y | 0.336 | 0.346 | 0.3776 | 0.048 | 0.084 | 0.040 | 0.094 | 0.072 | 0.126 | 0.128 | 0.139 | 0.174 |
| Zr | 0.328 | 0.335 | 0.3545 | 0.054 | 0.076 | 0.049 | 0.083 | 0.068 | 0.102 | 0.119 | 0.126 | 0.148 |
| Nb | 0.323 | 0.327 | 0.3383 | 0.058 | 0.071 | 0.055 | 0.075 | 0.066 | 0.086 | 0.113 | 0.117 | 0.130 |
| Mo | 0.320 | 0.323 | 0.3302 | 0.060 | 0.068 | 0.058 | 0.071 | 0.065 | 0.078 | 0.110 | 0.113 | 0.121 |
| Pd | 0.319 | 0.322 | 0.3279 | 0.060 | 0.067 | 0.059 | 0.070 | 0.065 | 0.076 | 0.109 | 0.112 | 0.119 |
| Ag | 0.322 | 0.326 | 0.3360 | 0.058 | 0.070 | 0.056 | 0.074 | 0.066 | 0.084 | 0.112 | 0.116 | 0.128 |
| Pt | 0.320 | 0.322 | 0.3297 | 0.060 | 0.068 | 0.058 | 0.070 | 0.065 | 0.078 | 0.110 | 0.113 | 0.121 |
| Au | 0.322 | 0.326 | 0.3360 | 0.058 | 0.070 | 0.056 | 0.074 | 0.066 | 0.084 | 0.112 | 0.116 | 0.128 |
| La | 0.339 | 0.350 | 0.3857 | 0.046 | 0.087 | 0.037 | 0.098 | 0.073 | 0.134 | 0.131 | 0.144 | 0.183 |

elemental addition:

$$TiFe_{0.962}M_{0.038} \ (1.9 \ at\% \ M)$$

$$TiFe_{0.874}M_{0.126} \ (6.3 \ at\% \ M)$$

$$TiFe_{0.750}M_{0.250} \ (12.5 \ at\% \ M)$$

Calculated lattice parameters, octahedral and tetrahedral sizes are displayed in Table 5 for various alloying additions. In a pure TiFe phase with a CsCl structure, titanium is located at the unit cell centre while Fe atoms are on the corners. This structure has a calculated lattice parameter of 0.315 nm and octahedral and tetrahedral diameters of 0.063 and 0.104 nm respectively. TiFe has an experimental lattice parameter of 0.297 nm [2] which is approximately 95% of the calculated value. In ternary systems with 12.5 at% additions, calculated lattice parameters range from 0.312 for alloying with Ni to 0.385 nm for alloying with La. For systems with M = 1.9 and 6.3 at%, all lattice parameters exceed the calculated lattice parameter of 0.315 nm, with the exception of Ni and Co.

Increasing M alloying content (except for Ni and Co) increases the lattice parameter but there is no uniform effect on the interstitial site size for the elements investigated. The interstitial site sizes vary for all additions according to $T > O_{Fe-Fe} > O_{M-Fe}$ except Ni and Co. The smaller atomic radii of Ni and Co (0.124 and 0.125 nm respectively) compared to Fe lead to the following interstitial site size order $T > O_{M-Fe} > O_{Fe-Fe}$. While $O_{Fe-Fe}$ remains the same or increases (for most additions), $O_{M-Fe}$ decreases by increasing M alloy content from 1.9 to 6.3 at%. Increasing M alloy content from 6.3 to 12.5 at%, causes both $O_{Fe-Fe}$ and $O_{M-Fe}$ to increase.

Hydrogen atoms prefer to occupy the largest sites to minimise strain energy and when the alloy is exposed to hydrogen, interstitial sites with the lowest strain energy will be filled first [14]. An empirical model was developed by Westlake [46] where the minimum H-H distance was 0.21 nm, suggesting some interstitial sites will remain empty due to the mutual repulsion of hydrogen. In addition, the minimum hole size for hydrogen occupancy was determined to be 0.04 nm. All calculated site sizes are either equal or exceed this value. Based on calculated sizes alone, hydrogen should first occupy tetrahedral sites, followed by $O_{Fe-Fe}$ then $O_{M-Fe}$. In pure BCC metals, such as V, tetrahedral interstices are the preferred site for hydrogen occupancy [47]. However, previous neutron diffraction measurements show most of the deuterium is in octahedral interstices

surrounded by two iron and four titanium atoms [48]. Tetrahedral sites are $Ti_2Fe_2$ polyhedrals whereas octahedral interstices are either $Ti_4Fe_2$ or $Ti_2Fe_4$ polyhedra. Since titanium is the main hydride forming element in TiFe based systems, in terms of bonding, it is reasonable that hydrogen prefers $O_{Fe-Fe}$ sites. With consideration of the above, the preferred hydrogen site occupation order is as follows: $O_{Fe-Fe}$, $O_{M-Fe}$. T sites. Fischer et al. [48] estimated 90% of deuterium atoms were located at (y, 0, 0) and the remaining 10% at (¼, ¼, y) in the TiFe unit cell where y is approximately ½ and both sites are $O_{Fe-Fe}$. Changes in the preferred hydrogen occupation sites were also reported for single and multicomponent metal hydride structures due to the increased hydrogen concentration and the formation of superabundant vacancies [49]–[51]. Hydrogen induces the formation of vacancies within the structure by reducing the vacancy formation energy [52]. It was demonstrated that the existence of vacancies will promote the occupation of octahedral sites, even at low hydrogen concentrations [50]. Therefore, accounting for interstitial site size alone is inadequate, and metal-hydrogen interactions must also be considered.

Fig. 2 also shows a scatter plot of calculated lattice parameters for 5 at% additions against plateau pressures of $TiFe_{0.9}M_{0.1}$ available in the literature. Unlike the TiFe system where the plateau pressure depends directly on B2 TiFe phase lattice parameters, there is not an obvious trend in the ternary system and most compositions have
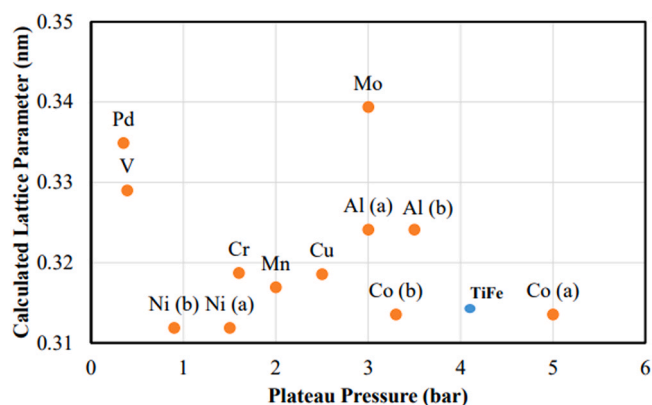


**Fig. 2.** Relationship between calculated lattice parameters for $TiFe_{0.9}M_{0.1}$ and desorption plateau pressure (β phase). Data from: Al (a), Co (a), Ni (a) [14]; Al (b) [4]; Co (b), Cr, Cu [17]; Mn [22]; Ni (b) [2]; Pd [40]; V [18].
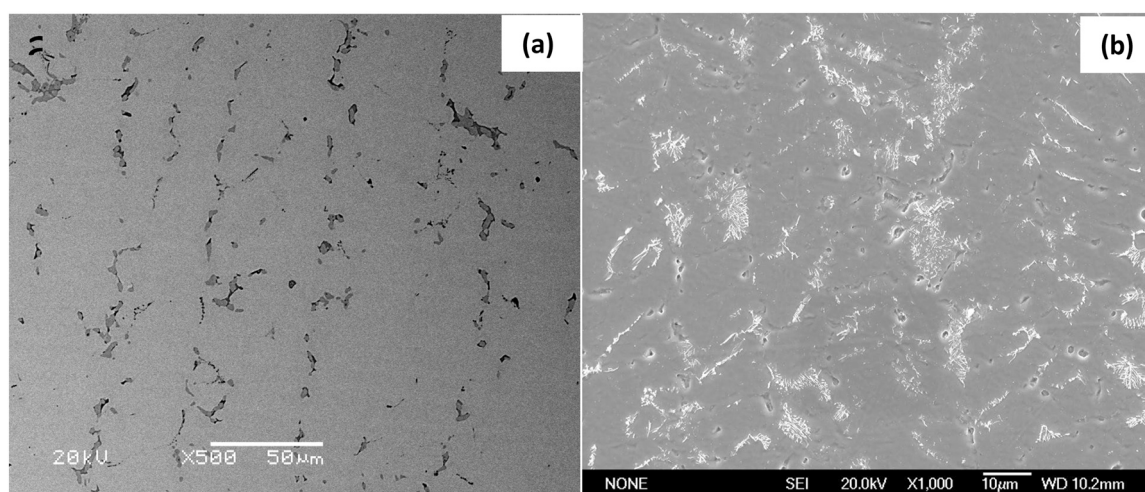
**Fig. 3.** Secondary electron micrograph of as-cast alloys 2 V (a) 5Zr (b).

plateau pressures below that for TiFe, including Co and Ni which had slightly smaller lattice parameters. The predictions of ternary plateau pressures for TiFe$_{0.96}$M$_{0.04}$ compositions [53] were moderately correlated with experimental values and found to be influenced directly by bond order (a measure of covalent bond strength).

For alloying additions that are also hydride formers, such as La, V and Y, it is also possible that a slightly higher proportion of hydrogen would occupy O$_{M-Fe}$ rather than O$_{Fe-Fe}$. The effect of alloying on TiFe electronic structure demonstrated [53] hydrogen atoms had greater affinity for Fe rather than Ti. The bond orders of Fe-H and M-H were larger than Ti-H, with M-H bond order increasing along each row of the periodic table. This further confirms that interstitial site size must be considered along with electronic structure as hydride stability also strongly depends on the chemical bonds between hydrogen and the atoms contained within the interstitial structure.

Therefore, in designing ternary TiFe-based alloys the interaction of several factors such as metal hydrogen bond dissociation energy, lattice parameters and interstitial hole size variation with additional elements, the tendency of additional elements to form intermetallic phases, and oxygen content should be concurrently considered. Based on these criteria, we study the effects of Zr (M-H bond dissociation energy: 221.7 kJ mol$^{-1}$, does not form intermetallic with Ti and a strong oxide former reacting preferentially with oxygen in the system) and V (M-H bond dissociation energy: 209.3 kJ mol$^{-1}$, does not form intermetallic with Ti) additions on the phase composition, structure, and hydrogen storage characteristics of the Ti-Fe-M alloys.

### 3.2. Compositional and structural analysis of cast alloys

Compositional analysis of the ternary alloys is given in Table 3. All compositions are slightly rich in titanium and iron deficient compared to their intended compositions. Ti-Fe-V alloys were relatively richer in vanadium while Ti-Fe-Zr alloy had slight zirconium deficiency.

Microstructural analysis conducted using SEM showed that all alloys consisted of three phases, Ti-Fe-V alloys (Fig. 3a for alloy 2 V) had a majority grey phase with two dark interdendritic phases, one with a globular morphology. Ti-Fe-Zr alloy (Fig. 3b) consisted mostly of a grey phase and two minor phases (dark and bright), both of which appeared to form interdendritically. Compositions and compositional ratios of these phases taken from point EDS measurements are shown in Table 6. Vanadium was present in small quantities in the grey phase of Ti-Fe-V alloys (2–4 V). This phase became richer in vanadium with increasing alloy vanadium content but maintained its Ti/Fe ratio of approximately 1:0.97. Most of the

**Table 6**
Individual phase compositions of Ti-Fe-V/Zr alloys measured by EDS, all in at% (EDS errors within ± 1 at%).

| Alloy | Phase | Ti | Fe | V or Zr | Ti/Fe/V or Zr Ratio |
|---|---|---|---|---|---|
| **2 V** | **Grey** | 49.66 | 49.09 | 1.25 | 1:0.99:0.03 |
| | **Dark** | 73 | 24 | 3 | 1:0.33:0.04 |
| | **Dark Grey** | 63.26 | 33.68 | 3.06 | 1:0.53:0.05 |
| **3 V** | **Grey** | 49.19 | 47.92 | 2.88 | 1:0.97:0.06 |
| | **Dark** | 70 | 24 | 6 | 1:0.34:0.08 |
| | **Dark Grey** | 60.83 | 33.28 | 5.89 | 1:0.55:0.1 |
| **4 V** | **Grey** | 48.02 | 46.58 | 5.41 | 1:0.97:0.11 |
| | **Dark** | 68 | 26 | 6 | 1:0.37:0.09 |
| | **Dark Grey** | 61 | 29 | 10 | 1:0.47:0.17 |
| **5Zr** | **Grey** | 50.13 | 49.71 | 0.16 | 1:0.99:0 |
| | **Dark** | 96.30 | 3.65 | 0.06 | 1:0.04:0 |
| | **Bright** | 50.52 | 40.12 | 9.36 | 1:0.79:0.19 |

added vanadium was contained in the two minor phases (dark and dark grey). Dark precipitates were richer in titanium than dark grey precipitates, with average Ti/Fe ratios of 1:0.35 and 1:0.5 respectively. Zirconium was present in small quantities in the grey and dark phases however, the majority was in the bright phase (9.36 at%). Relative to the Ti-Fe-V system, the dark phase in Ti-Fe-Zr alloy was very rich in titanium, with 96.30 at% Ti. XRD pattern of alloys 3 V and 5Zr are shown in Fig. 4 along with the Binary TiFe alloy. The B$_2$ TiFe is observed in all alloy compositions and is the dominant phase while a small amount of FCC Ti$_4$Fe$_2$O is also observed in alloys 3 V and 4 V. With consideration of results from individual phase EDS and XRD, the following phases are most likely in Ti-Fe-V/Zr alloys: grey phase-B2 TiFe, and dark grey-FCC Ti$_4$Fe$_2$O. The titanium-rich dark phase was not detected using XRD, probably due to its small quantity XRD peaks were not seen for the bright phase in Ti-Fe-Zr alloy so the structure is unknown. A bright phase with a similar composition was previously identified [35] and broadly suggested to be the HCP Ti$_{0.8}$Fe$_{0.2}$Zr$_{0.2}$ phase.

XRD patterns were used to identify lattice parameters, unit cell volume and volume fraction of the phases which the results of are shown in Table 7. B2 TiFe cell volume rises approximately linearly from 26.48 Å$^3$ in alloy 2 V to 26.78 Å$^3$ in alloy 4 V. EDS results support this trend as phase vanadium content increases from 1.25 to 5.41 at% while iron content decreases from 49.09 to 46.58 at% (Table 6). Since vanadium has a larger atomic radius (205 pm) than iron (126 pm), a larger unit cell volume is expected. B2 TiFe cell volumes of Ti-Fe-V alloys are in line with the reported values of 26.64 and 26.71 Å$^3$ for TiFe$_{0.9}$V$_{0.05}$ and TiFe$_{0.9}$V$_{0.1}$ respectively [18]. The unit cell volume of B2 TiFe for alloy Ti-Fe-Zr (26.83 Å$^3$) is slightly
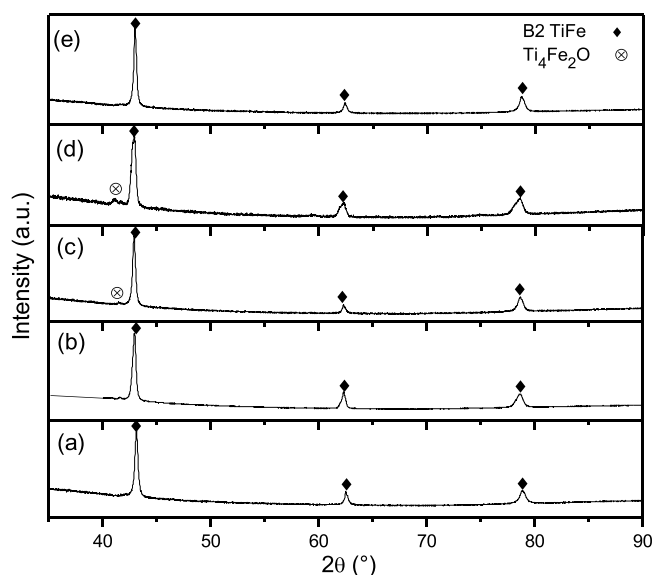
**Fig. 4.** X-ray diffraction scans of alloys 1 (a), 2–4 V (b-d), and 5Zr (e) in the as-cast state.

**Table 7**

Crystal structure refinement results using Rietveld method for Ti-Fe-V/Zr alloys containing B2 TiFe, FCC $Ti_4Fe_2O$.

| Alloy | Phase | Lattice Parameters (Å) | | Unit Cell Volume (Å$^3$) | Volume fraction |
|-------|-------|---|---|---|---|
| **1** | **B2 TiFe** | **a** | 2.97 | 26.35 | 1 |
| **2 V** | **B2 TiFe** | **a** | 2.98 | 26.48 | 1 |
| **3 V** | **B2 TiFe** | **a** | 2.98 | 26.62 | 0.911 |
| | **FCC Ti₄Fe₂O** | **a** | 11.29 | 1440 | 0.089 |
| **4 V** | **B2 TiFe** | **a** | 2.99 | 26.78 | 0.786 |
| | **FCC Ti₄Fe₂O** | **a** | 11.41 | 1489 | 0.214 |
| **5Zr** | **B2 TiFe** | **a** | 2.99 | 26.83 | 1 |

higher compared to the literature values of 26.47 – 26.54 Å$^3$ [16], [25].

Increasing alloy vanadium from 3.2 to 6.5 at% led to an expansion of FCC $Ti_4Fe_2O$ cell volume from 1440 to 1489 Å$^3$ in alloys 3 V and 4 V respectively (Table 7). However, it was shown that [18] the unit cell volume of FCC $Ti_4Fe_2O$ remains at approximately 1440 Å$^3$ after increasing the vanadium content from 5.6 to 8.9 at%. The increase in vanadium was probably offset by a decrease in phase titanium content (61.4–58.2 at%) whereas, in this study, FCC $Ti_4Fe_2O$ titanium content increased from 60.8 to 61 at% in alloys 3 V and 4 V respectively.

### 3.3. Hydrogen storage characteristics

Hydrogen storage isotherms measured for Ti-Fe-V and Ti-Fe-Zr alloys are shown in Figs. 5a and 5b respectively, along with alloy 1 for comparison. Alloys modified by V and particularly with Zr were significantly easier to activate compared to the binary alloy (Table 4). A summary of storage characteristics obtained from isothermal measurements is shown in Table 8. Isotherm shapes of alloys 2 V, 3 V and 5Zr are comparable to alloy 1 where two plateaux, β and γ, can be seen, of which γ is significantly sloped occurring at higher pressures.

There have been no systematic investigations into the effects of composition on plateau slope in B2 TiFe alloys. The addition of vanadium increases the plateau slope in Ti-Mn-V alloys compared to the binary alloy. However, both an increase in the V content and a decrease in the Ti content of B2 TiFe phase reduce the plateau slope in Ti-Fe-V alloys.

The plateau slope in Ti-Fe-Zr alloy is comparable to alloy 1 and changes with zirconium content are difficult to determine as only one Ti-Fe-Zr composition was considered in this study. In addition to the alloy composition, plateau slope is also sensitive to strain effects [55], which refers to the size difference between titanium atoms and those of the alloying addition. A greater mismatch between these leads to local distortions and higher strain within the B2 TiFe matrix and changes in interstice sizes. Hole size calculations in Table 5 showed octahedral and tetrahedral radii were larger with vanadium compared to the binary alloy. Differences in the interstice sizes may explain the higher slope observed in Ti-Fe-V alloys. Other studies examining the Ti-Fe-Zr [36,54] showed highly sloped plateaux however, the amount of zirconium added was significantly higher than this study (0.15 at% compared to minimum of 2.5 at% Zr). EDS measurements of B2 TiFe (Table 6) confirmed vanadium was substituting for iron in Ti-Fe-V alloys. Vanadium has a higher affinity for hydrogen than iron, therefore is expected to increase the hydrogen capacity. Table 8 confirms the positive effect of vanadium for increasing the maximum and more significantly the reversible hydrogen capacities in Ti-Fe-V alloys as a function of B2 TiFe phase vanadium content (Table 6).

Thermodynamic data of hydrogen absorption for the studied alloys were obtained from the Van't Hoff plots which are summarised in Table 8. Similar to the TiFe alloy, plateau pressure seems to be directly related to the B2 TiFe phase lattice parameter (Tables 7 and 8) in Ti-Fe-V alloys, indicating the adjustment of B2 TiFe composition as a suitable method for tuning the thermodynamic of each ternary alloys.
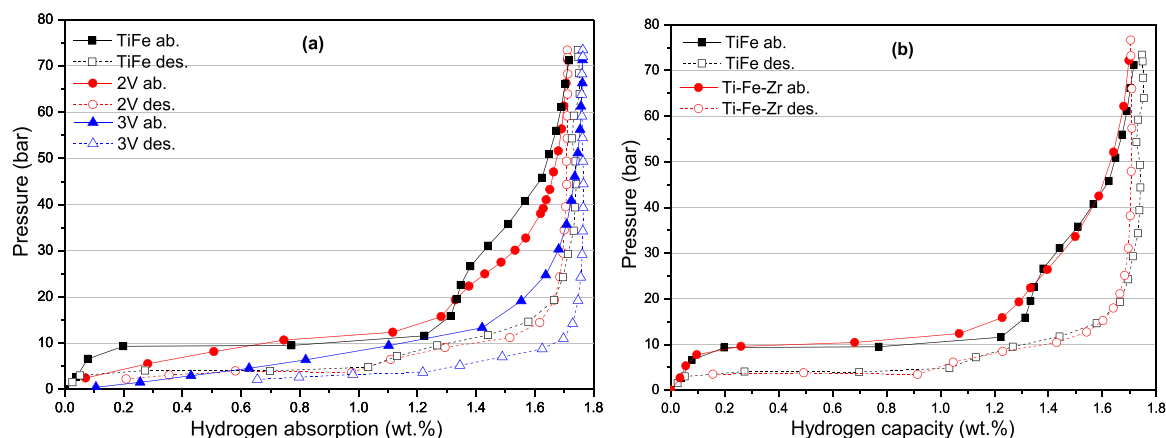


**Fig. 5.** PCIs of alloys 1, 2 V and 3 V (a). PCIs of alloys 1 and 5Zr (b) all measured at room temperature.

**Table 8**
Room temperature isotherm characteristics measured of alloys 2 V, 3 V, and 5Zr. Results for alloy 1 are included for comparison.

| Alloy | Maximum capacity (wt% H) | Reversible capacity (wt% H) | Absorption plateau (bar) | Desorption Plateau (bar) | Hysteresis ln $(P_{abs}/P_{des})$ | Absorption Slope ln $(P_{max}/P_{min})$ | $\Delta H$ (kJ mol$^{-1}$ H$_2$) | $\Delta S$ (J mol$^{-1}$ K$^{-1}$ H$_2$) |
|---|---|---|---|---|---|---|---|---|
| **1** | 1.75 | 1.19 | 10.9 | 4.1 | 0.99 | 1.25 | -23.02 | 98.15 |
| **2 V** | 1.74 | 1.20 | 9.1 | 4.6 | 0.68 | 2.14 | -16.80 | 75.20 |
| **3 V** | 1.76 | 1.42 | 6.9 | 2.7 | 0.95 | 1.94 | -25.75 | 100.48 |
| **5Zr** | 1.71 | 1.22 | 11.0 | 3.6 | 1.12 | 1.27 | -20.59 | 89.38 |

## 4. Conclusions

TiFe-based ternary alloys (Ti-Fe-V and Ti-Fe-Zr) were fabricated based on the evaluation of several design criteria such as the effects of additional elements on the maximum hydrogen storage capacity with respect to their bond dissociation energy, their capability to form intermetallic phases, susceptibility to form oxide phases, and their influences on the interstitial site sizes and hydride stability.

Hydrogen storage characteristics of the fabricated alloys were examined, and it was shown that vanadium addition led to higher reversible capacities in both alloys 2 V and 3 V but maximum capacity remined almost similar. Increased hydrogen storage capacities was attributed to the V substitution for Fe, with a higher affinity to hydrogen. Hydrogen storage characteristics of Ti-Fe-Zr alloy were comparable to the TiFe alloy, likely due to the small amount of zirconium added (0.15 at%) and limited solubility of zirconium in the B2 TiFe phase. However, the main advantage of this alloy was significantly easier activation. Lower plateau pressures were seen for Ti-Fe-V alloys with increasing lattice parameters. Plateau slope increased in alloys 2 V and 3 V compared to the binary alloy but decreased as a function of B2 TiFe phase vanadium content in Ti-Fe-V alloys, demonstrating the effect of B2 TiFe phase lattice parameter on the thermodynamic properties of the ternary alloys. Our results reveal the importance of considering various design parameters for the development of TiFe-based ternary (or multiparty) alloys as the hydrogen storage characteristics of the alloys are imposed by the interplay between such parameters.

## CRediT authorship contribution statement

**Shahrouz Nayebossadri**: Conceptualisation, Methodology, Validation, Formal analysis, Writing – original draft, Visualisation, Writing – review & editing. **Carmel Jenjira Greenwood:** Conceptualisation, Methodology, Investigation, Formal analysis. **David Book:** Review, Funding acquisition.

## Data Availability

Data will be made available on request.

## Declaration of Competing Interest

The authors declare that they have no known competing financial interests or personal relationships that could have appeared to influence the work reported in this paper.

## Appendix A. Supporting information

Supplementary data associated with this article can be found in the online version at doi:10.1016/j.jallcom.2023.169456.

## References

[1] P. Thompson, J.J. Reilly, F. Reidinger, J.M. Hastings, L.M. Corliss, Neutron diffraction study of gamma iron titanium deuteride, J. Phys. F. Met. Phys. vol. 9, (4) (1979), https://doi.org/10.1088/0305-4608/9/4/001

[2] J.J. Reilly, R.H. Wiswall, Formation and properties of iron titanium hydride, Inorg. Chem. vol. 13, (1) (1974) 218–222, https://doi.org/10.1021/ic50131a042

[3] H. Liu, J. Zhang, P. Sun, C. Zhou, Y. Liu, Z.Z. Fang, Effect of oxygen on the hydrogen storage properties of TiFe alloys, J. Energy Storage vol. 55, (PB) (2022) 105543, , https://doi.org/10.1016/j.est.2022.105543

[4] J.R. Sandrock, G.; Reilly, J.J.; Johson, Metallurgical considerations in the production and use of FeTi alloys for hydrogen storage 1976, pp. 965–971.

[5] L. Schlapbach, T. Riesterer, The activation of FeTi for hydrogen absorption, Appl. Phys. A Solids Surf. vol. 32, (4) (1983) 169–182, https://doi.org/10.1007/BF00820257

[6] T. Schober, D.G. Westlake, The activation of FeTi for hydrogen storage: a different view, Scr. Metall. vol. 15, (8) (1981) 913–918, https://doi.org/10.1016/0036-9748(81)90277-5

[7] K. Edalati, J. Matsuda, A. Yanagida, E. Akiba, Z. Horita, Activation of TiFe for hydrogen storage by plastic deformation using groove rolling and high-pressure torsion: similarities and differences, Int. J. Hydrog. Energy vol. 39, (28) (2014) 15589–15594, https://doi.org/10.1016/j.ijhydene.2014.07.124

[8] H. Emami, K. Edalati, J. Matsuda, E. Akiba, Z. Horita, Hydrogen storage performance of TiFe after processing by ball milling, Acta Mater. vol. 88, (2015) 190–195, https://doi.org/10.1016/j.actamat.2014.12.052

[9] K. Edalati, E. Akiba, Z. Horita, High-pressure torsion for new hydrogen storage materials, Sci. Technol. Adv. Mater. vol. 19, (1) (2018) 185–193, https://doi.org/10.1080/14686996.2018.1435131

[10] A. Venkert, M. Talianker, M.P. Dariel, A tem study of activated FeTi surface, Mater. Lett. vol. 2, (1) (1983) 45–48, https://doi.org/10.1016/0167-577X(83)90030-7

[11] T. Schober, On the activation of FeTi for hydrogen storage, J. Less-Common Met vol. 89, (1) (1983) 63–70, https://doi.org/10.1016/0022-5088(83)90249-7

[12] T. Matsumoto, M. Amano, Y. Sasaki, Hydrogenation of FeTi-based alloys containing β-Ti, J. Less-Common Met vol. 88, (2) (1982) 443–449, https://doi.org/10.1016/0022-5088(82)90255-7

[13] T. Mizuno, T. Morozumi, Titanium concentration in FeTix (1 ≤ x ≤ 2) alloys and its effect on hydrogen storage properties, J. Less-Common Met. vol. 84, (C) (1982) 237–244, https://doi.org/10.1016/0022-5088(82)90148-5

[14] S.M. Lee, T.P. Perng, Correlation of substitutional solid solution with hydrogenation properties of TiFe 1 2, J. Alloy. Compd. vol. 291, (1999) 254–261.

[15] G. Bruzzone, G. Costa, M. Ferretti, G.L. Olcese, Hydrogen storage in aluminium-substituted TiFe compounds, Int. J. Hydrog. Energy vol. 6, (2) (1981) 181–184, https://doi.org/10.1016/0360-3199(81)90006-9

[16] R. Suzuki, J. Ohno, H. Gondoh, Effect of sulphur addition on the properties of FeTi alloy for hydrogen storage, J. Less-Common Met vol. 104, (1) (1984) 199–206, https://doi.org/10.1016/0022-5088(84)90455-7

[17] J.R. Reilly, J.J.; Johnson, Titanium alloy hydrides; their properties and applications, in 1st world Hydrogen Conference, 1976, pp. 8B3–8B26.

[18] A. Guéguen, M. Latroche, Influence of the addition of vanadium on the hydrogenation properties of the compounds TiFe0.9Vx and TiFe0.8Mn 0.1Vx (x = 0, 0.05 and 0.1), J. Alloy. Compd. vol. 509, (18) (2011) 5562–5566, https://doi.org/10.1016/j.jallcom.2011.02.036

[19] M. Someno, M. Arita, R. Kinaka, Y. Ichinose, Hydrogen absorption and hydriding of Ti-based intermetallic compounds, in hydrogen in Metals, Trans. Japn. Inst. Met. vol. 21, (1979) 325–328 (doi: https://doi.org/).

[20] M.H. Mintz, S. Vaknin, S. Biderman, Z. Hadari, Hydrides of ternary TiFexM1-x (M=Cr, Mn, Co, Ni) intermetallics alloys, J. Appl. Phys. vol. 52, (1981) 463–467.

[21] T. Yang, et al., Effect of chromium, manganese and yttrium on microstructure and hydrogen storage properties of TiFe-based alloy, Int. J. Hydrog. Energy vol. 45, (21) (2020) 12071–12081, https://doi.org/10.1016/j.ijhydene.2020.02.086

[22] S.V. Mitrokhin, V.N. Verbetsky, R.R. Kajumov, H. Cunmao, Z. Yufen, Hydrogen sorption peculiarities in FeTi-type TiFeVMn alloys, J. Alloy. Compd. vol. 199, (1–2) (1993) 155–160, https://doi.org/10.1016/0925-8388(93)90443-Q

[23] H. Qu, et al., Effects of Co introduction on hydrogen storage properties of Ti-Fe-Mn alloys, Int. J. Hydrog. Energy vol. 40, (6) (2015) 2729–2735, https://doi.org/10.1016/j.ijhydene.2014.12.089

[24] K. Edalati, et al., Impact of severe plastic deformation on microstructure and hydrogen storage of titanium-iron-manganese intermetallics, Scr. Mater. vol. 124, (2016) 108–111, https://doi.org/10.1016/j.scriptamat.2016.07.007

[25] P. Modi, K.F. Aguey-Zinsou, Titanium-iron-manganese (TiFe0.85Mn0.15) alloy for hydrogen storage: reactivation upon oxidation, Int. J. Hydrog. Energy vol. 44, (31) (2019) 16757–16764, https://doi.org/10.1016/j.ijhydene.2019.05.005

[26] A.K. Patel, A. Duguay, B. Tougas, C. Schade, P. Sharma, J. Huot, Microstructure and first hydrogenation properties of TiFe alloy with Zr and Mn as additives, Int. J. Hydrog. Energy vol. 45, (1) (2020) 787–797, https://doi.org/10.1016/j.ijhydene.2019.10.239

[27] H. Suzuki, Y. Osumi, A. Kato, K. Oguro, M. Nakane, Hydrogen absorption-desorption characteristics of Ti-Co-Fe Alloys, J. Less-Common Met vol. 80, (2) (1981) 179–185, https://doi.org/10.1016/0022-5088(81)90091-6

[28] H. Miyamura, M. Takada, K. Hirose, S. Kikuchi, Metal hydride electrodes using titanium-iron-based alloys, J. Alloy. Compd. vol. 356–357, (2003) 755–758, https://doi.org/10.1016/S0925-8388(03)00084-7

[29] R. Wakabayashi, N. Yasuda, S. Sasaki, N. Okinaka, T. Akiyama, Self-ignition combustion synthesis of TiFe1-xNix in hydrogen atmosphere, J. Alloy. Compd. vol. 484, (1–2) (2009) 682–688, https://doi.org/10.1016/j.jallcom.2009.05.022

[30] Y. Li, H. Shang, Y. Zhang, P. Li, Y. Qi, D. Zhao, Investigations on gaseous hydrogen storage performances and reactivation ability of as-cast TiFe1-xNix (x=0, 0.1, 0.2 and 0.4) alloys, Int. J. Hydrog. Energy vol. 44, (8) (2019) 4240–4252, https://doi.org/10.1016/j.ijhydene.2018.12.144

[31] P. Jain, C. Gosselin, J. Huot, Effect of Zr, Ni and Zr7Ni10 alloy on hydrogen storage characteristics of TiFe alloy, Int. J. Hydrog. Energy vol. 40, (47) (2015) 16921–16927, https://doi.org/10.1016/j.ijhydene.2015.06.007

[32] C. Gosselin, J. Huot, First hydrogenation enhancement in TiFe alloys for hydrogen storage doped with yttrium, Metals vol. 9, (2) (2019) 1–10, https://doi.org/10.3390/met9020242

[33] N. Nishimiya, T. Wada, A. Matsumoto, K. Tsutsumi, Hydriding characteristics of zirconium-substituted FeTi, J. Alloy. Compd. vol. 313, (1–2) (2000) 53–58, https://doi.org/10.1016/S0925-8388(00)01181-6

[34] P. Lv, J. Huot, Hydrogen storage properties of Ti0.95FeZr0.05, TiFe0.95Zr0.05 and TiFeZr0.05 alloys, Int. J. Hydrog. Energy vol. 41, (47) (2016) 22128–22133, https://doi.org/10.1016/j.ijhydene.2016.07.091

[35] C. Gosselin, J. Huot, Hydrogenation properties of TiFe doped with zirconium, Materials vol. 8, (11) (2015) 7864–7872, https://doi.org/10.3390/ma8115423

[36] P. Lv, Z. Liu, Effect of high zirconium content on hydrogenation properties and anti-poisoning ability of air-exposed TiFe alloy, J. Mater. Res. Technol. vol. 8, (6) (2019) 5972–5983, https://doi.org/10.1016/j.jmrt.2019.09.072

[37] A.K. Patel, B. Tougas, P. Sharma, J. Huot, Effect of cooling rate on the microstructure and hydrogen storage properties of TiFe with 4 wt% Zr as an additive, J. Mater. Res. Technol. vol. 8, (6) (2019) 5623–5630, https://doi.org/10.1016/j.jmrt.2019.09.030

[38] Y. Sasaki, M. Amano, Hydrogen storage properties of Fe1-xNbxTi, Hydrogen Energy Progress, Pergamon, 1981.

[39] H. Nagai, M. Nakatsu, K. Shoji, H. Tamura, Effect of simultaneous addition of oxygen with copper or niobium on the hydriding characteristics ofFeTiF or hydrogen storage, J. less vol. 119, (1986) 131–142.

[40] I. Yamashita, H. Tanaka, H. Takeshita, N. Kuriyama, T. Sakai, I. Uehara, Hydrogenation characteristics of TiFe1 - XPdx (0.05≤x≤0.30) alloys, J. Alloy. Compd. vol. 253–254, (1997) 238–240, https://doi.org/10.1016/S0925-8388(96)02925-8

[41] H. Miyamura, M. Takada, S. Kikuchi, Characteristics of hydride electrodes using Ti-Fe-Pd-X alloys, J. Alloy. Compd. vol. 404–406, (SPEC. ISS) (2005) 675–678, https://doi.org/10.1016/j.jallcom.2005.03.098

[42] X. Wang, R. Chen, C. Chen, Q. Wang, Hydrogen storage properties of TixFe + y wt % La and its use in metal hydride hydrogen compressor, J. Alloy. Compd. vol. 425, (1–2) (2006) 291–295, https://doi.org/10.1016/j.jallcom.2006.01.025

[43] A. Coelho, Topas-Academic, Version 4.1, Coelho Software, Brisbane, Australia, 2007.

[44] C.E. Lundin, F.E. Lynch, C.B. Magee, A correlation between the interstitial hole sizes in intermetallic compounds and the thermodynamic properties of the hydrides formed from those compounds, J. Less-Common Met vol. 56, (1) (1977) 19–37, https://doi.org/10.1016/0022-5088(77)90215-6

[45] C.J. Greenwood, Development of TiFe-based alloys for stationary hydrogen storage applications, University of Birmingham, 2020.

[46] D.G. Westlake, Site occupancies and stoichiometries in hydrides of intermetallic compounds: geometric considerations, J. Less-Common Met vol. 90, (2) (1983) 251–273, https://doi.org/10.1016/0022-5088(83)90075-9

[47] Y. Fukai, Site preference of interstitial hydrogen in metals, J. Less Common Met vol. 101, (1984) 1–16, https://doi.org/10.1002/9783527678679.dg12070

[48] P. Fischer, W. Hälg, L. Schlapbach, F. Stucki, A.F. Andresen, Deuterium storage in FeTi. Measurement of desorption isotherms and structural studies by means of neutron diffraction, Mater. Res. Bull. vol. 13, (9) (1978) 931–946, https://doi.org/10.1016/0025-5408(78)90105-8

[49] Y. Fukai, Y. Shizuku, Y. Kurokawa, Superabundant vacancy formation in Ni-H alloys, J. Alloy. Compd. vol. 329, (1–2) (2001) 195–201, https://doi.org/10.1016/S0925-8388(01)01603-6

[50] C.M. Moore, J.A. Wilson, M.J.D. Rushton, W.E. Lee, J.O. Astbury, S.C. Middleburgh, Hydrogen accommodation in the TiZrNbHfTa high entropy alloy, Acta Mater. vol. 229, (2022) 117832, , https://doi.org/10.1016/j.actamat.2022.117832

[51] H. Koike, Y. Shizuku, A. Yazaki, Y. Fukai, Superabundant vacancy formation in Nb-H alloys; resistometic studies, J. Phys. Condens. Matter vol. 16, (8) (2004) 1335–1349, https://doi.org/10.1088/0953-8984/16/8/017

[52] M.L. Fullarton, R.E. Voskoboinikov, S.C. Middleburgh, Hydrogen accommodation in α-iron and nickel, J. Alloy. Compd. vol. 587, (2014) 794–799, https://doi.org/10.1016/j.jallcom.2013.10.169

[53] H. Yukawa, Y. Takahashi, M. Morinaga, Electronic structures of hydrogen storage compound, TiFe, Comput. Mater. Sci. vol. 14, (1–4) (1999) 291–294, https://doi.org/10.1016/s0927-0256(98)00121-9

[54] P. Jain, C. Gosselin, N. Skryabina, D. Fruchart, J. Huot, Hydrogenation properties of TiFe with Zr7Ni10 alloy as additive, J. Alloy. Compd. vol. 636, (2015) 375–380, https://doi.org/10.1016/j.jallcom.2015.02.104

[55] J.M. Park, J.Y. Lee, Effect of alloying element on the sloping hydrogen plateaux in zirconium-based laves phase systems, J. Alloy. Compd. vol. 182, (1) (1992) 43–54, https://doi.org/10.1016/0925-8388(92)90572-Q

[59] T.L. COTTRELL, The strength of chemical bonds, 2nd ed., Butterworth, London, 1958.

[60] Y.R. Luo, Comprehensive Hnadbook of Chemical Bond Energies, 1st ed. 2007.